https://doi.org/10.5194/acp-2021-407
Preprint. Discussion started: 31 May 2021

Atmospheric Chemistry and Physics Discussions

Anthropogenic Aerosol effects on Tropospheric Circulation and Sea Surface Temperature (1980-2020): Separating the role of Zonally Asymmetric Forcings

Chenrui Diao [1], Yangyang Xu [1,*], Shang-Ping Xie [2]

[1] Department of Atmospheric Sciences, Texas A&M University, College Station, Texas 77843, USA
[2] Scripps Institute of Oceanography, University of California, San Diego, La Jolla, CA 92093, USA

Correspondence to: Yangyang Xu (yangyang.xu@tamu.edu)

https://doi.org/10.5194/acp-2021-407
Preprint. Discussion started: 31 May 2021

Atmospheric Chemistry and Physics Discussions

Abstract. Anthropogenic Aerosols (AA) induce global and regional tropospheric circulation adjustments due to the radiative energy perturbations. The overall cooling effects of AA since the pre-industrial (PI) era, to mask a portion of global warming, have been the subject of many studies with large uncertainty remaining. The interhemispheric contrast in AA forcing has also been demonstrated to induce a major shift in atmospheric circulation. The zonally heterogeneous changes in AA emissions since the late 20th century, with a notable decline in the Western Hemisphere and continuous increase in the Eastern Hemisphere, received less attention. Here we utilize four sets of single-model initial-condition large-ensemble simulations with various combinations of external forcings to quantify the different radiative and circulation responses due to aerosol emissions changes during 1980-2020. In particular, we focus on the distinct climate responses to Fossil-Fuel (FF) related aerosol from Western Hemisphere (WH) versus Eastern Hemisphere (EH).

The zonal and meridional redistribution of FF aerosols from WH to EH results in negative radiative forcing over Asia and positive radiative forcing over North America and Europe. This leads to a counterclockwise anomaly of zonal mean stream function over the tropics (i.e. a northward shift of Hadley cell) and stronger equatorward shift of the Northern Hemisphere (NH) jet stream, consistent with the thermal wind argument with the gradient of surface air temperature (SAT) as a predictive metric.

Two sets of regional FF simulations (Fix_EastFF1920 and Fix_WestFF1920) are performed and reveals the dominating role of WH forcing due to aerosol reduction in the NH. The Aerosol reduction over WH mid-to-high latitudes dominates the warming over NH mid-to-high latitudes. The increased aerosol over the EH low-to-mid latitudes is confined more locally but also induces slight warming over the northeastern Pacific and North Atlantic. The competing role of FF forcing originating from EH and WH in shaping tropospheric circulation and surface climate response indicates the importance of both zonal and meridional distribution of aerosol forcing within the NH, and previous idealized models that only consider the zonal difference of aerosol emission may oversimplify the real aerosol forcing.

https://doi.org/10.5194/acp-2021-407
Preprint. Discussion started: 31 May 2021


Atmospheric Chemistry and Physics Discussions

1 Introduction

The external forcings due to anthropogenic activities and internal variabilities originating from the ocean-atmosphere system together determine climate change at decadal time scales (Kirtman et al., 2013; Meehl et al., 2013). Since the Industrial Revolution, the increasing GHG emissions have been shown to be the leading cause of global warming of about 1 ºC (as of the 2010s; IPCC, 2018). On the other hand, the internal variation of the climate, which fluctuates at time scales ranging from years to decades, modulate the paces of global warming at a shorter decal to a multidecadal time scale (Dai et al., 2015; Xie and Kosaka, 2017), also with regional implications such as sea ice retreat (Ding et al., 2019).

In addition to GHG forcing and internal variability, another major confounding factor affecting regional climate change at decadal scales is anthropogenic aerosol forcing. Despite decades of research into this subject, quantitative understandings of the regional climate effects of Anthropogenic Aerosols (AA) remain highly uncertain. There is still limited understanding of the physical mechanisms governing the strength of AA radiative forcing, for example, due to complex aerosol-cloud interaction (Bender, 2020), the brownness of organic aerosols (Bahadur et al., 2012; Jacobson, 2012; Kodros et al., 2015), surface albedo changes due to black carbon aerosols (Xu et al., 2016; Liu et al., 2020). Additionally, there are two more reasons why a robust attribution of past climate change to AA is difficult: uneven spatial distributions and fast temporal evolutions of emission/concentration/forcing. That is, unlike GHGs, the lifetimes of aerosols are as short as days, and thus the spatial distribution of aerosol concentration and its forcing is highly heterogeneous, which may perturb regional climate differently compared to the well-mixed GHG (Ming and Ramaswamy, 2011; Shindell et al., 2015). Lin et al. (2018) analyzed the relationship between aerosol and precipitation extremes and showed that precipitation extremes are more sensitive to aerosols than GHGs. Wang et al. (2020) showed a large shift in South Hadley circulation due to AA in the 20th century. Also, the relatively shorter lifetime means that AA concentrations respond to local emission changes quickly. Indeed, global sulfate aerosol concentration has declined following strengthened emission control measures in the developed nations in the West (Klimont et al., 2013), in contrast to the monotonic increase in GHG concentration since the industrial revolution. Recently, Wang et al. (2020) demonstrated that the reduced aerosol emission over Europe suppresses the Eurasia wintertime extremes. The decline of AA is likely to continue in the future (Andreae et al., 2005; Zheng et al., 2020), which is projected to intensify severe heat extremes (Zhao et al., 2019; Xu et al., 2020).

Because of the unique temporal and spatial features of AA, some have argued that the aerosol forcing can induce an external-forced “decadal variability”, which can then be imposed onto the natural variabilities, further confounding a robust attribution of observed changes at a shorter time scale. For example, several recent studies suggested the reduction in aerosol emission over Europe contributes to the Atlantic Multidecadal Variability, which is to a large part attributed to internal oceanic processes (Booth et al., 2012; Bellomo et al., 2018; Hua et al., 2019; Watanabe and Tatebe. 2019). Some studies focused on aerosol effects on the Pacific decadal to multidecadal variations, arguing that aerosol forcings can induce Pacific

https://doi.org/10.5194/acp-2021-407
Preprint. Discussion started: 31 May 2021


Atmospheric Chemistry and Physics Discussions

decadal variation (et al., 2014; Dong et al., 2014; Hua et al., 2018), but the relative contribution of external forcing and internal variability remains unclear.

Given the rapid temporal evolution of global aerosol emission, as well as the redistribution of dominant aerosol emission regions from the West to East, we need to address the question of how AA affects the decadal variations over Asia and the Pacific Ocean. Recent studies have compared the heterogeneous aerosol emission patterns and tried to explain how the climate responds to the competition of EH and WH aerosol emission. The regional warming due to the recent aerosol unmasking in the West can have profound implications on regional extremes (Samset et al., 2018; Zhao et al., 2019; Wang et al., 2020), Arctic sea ice (Krishnan et al., 2020), etc. Wang et al. (2015) demonstrated that the redistribution of aerosol from west to east induces a southward shift of circulation systems and the weakening of tropics circulation. Understanding the climate response to zonally asymmetric forcing is a main motivation of the present study because an improved understanding can help shed light on other relevant problems on regional forcings, such as land-use changes (e.g. deforestation over Amazon vs. Africa), volcanic eruption (Verma et al., 2019), geoengineering solutions such as stratospheric or tropospheric aerosol injection conducted over different locations, and the potential contrast of China and India's future emission trajectories in future decades (Samset et al., 2019; Wang et al., 2021).

The FF aerosol is projected to further decrease in future decades, even for Asian regions, with more strict air quality measurements in developing nations, and thus will lead to further unmasking and warming in addition to GHG-induced global warming (Xu et al., 2015; Wang et al., 2018; Lelieveld et al., 2019; Allen et al., 2020).

This study utilized a recently available large ensemble fully coupled global climate model simulation to assess the aerosol impact on global climate change in the past few decades (1980-2020). The present study focuses on the zonal (west to east) asymmetry of aerosol forcing within the Northern Hemisphere, We aim to detail how the upward EH AA emission trend and the downward WH AA trend competes to affect tropical and mid-latitude circulation, and simultaneously, affect the North Pacific surface climate which may have played a role in determining the observed Pacific decadal variations.

The structure of this paper is the following. In Sect. 2, we provide the details of the climate model, published simulation, and our new model experiment. In Sect. 3, we present simulated responses on the global and regional radiation(Sect. 3.1), air temperature (Sect. 3.2), and NH tropospheric circulation (Sect. 3.3) with a focus on separating the role of FF forcing over WH and EH with clear zonal asymmetry. The Importance of the latitudinal distribution of AA forcing in driving Pacific temperature change is discussed in Sect. 3.4. In Sect. 4, we summarize our findings and suggest scientific questions for future research.

https://doi.org/10.5194/acp-2021-407
Preprint. Discussion started: 31 May 2021


Atmospheric Chemistry and Physics Discussions

2 Methods

2.1 Climate model

The climate model used in this study is the Community Earth System Model 1 (CESM1). CESM1 is a fully coupled model developed by NCAR and community scientists (Hurrell et al., 2014) and is one of the models participating in the Coupled Model Intercomparison Project Phase 5 (CMIP5) (Meehl et al., 2016). The CESM1 has been extensively applied in a variety of climate studies including the ones focusing on external forcing and internal variability (e.g., Swart et al., 2015; Xu et al., 2015; Kay et al., 2015; Ding et al., 2019). Studies utilizing CMIP5 multi-model comparison (e.g., Samset et al., 2016; Smith et al., 2016; Lin et al., 2018) also demonstrated its capability for attribution studies on human-induced regional climate change.

Relevant to the aerosol effect focused on this study, a scheme of the three-mode aerosol model (MAM3) - Aitken, accumulation, and coarse modes (Liu et al., 2012), is used by default in CESM1 (CAM5). Aerosol concentration (including sulfates, black carbons, organic carbons) in CESM1 (CAM5) is calculated online from the historical (up to 2005) and future (RCP8.5 thereafter) emission scenarios. The cloud physics scheme allows ice supersaturation and features activation of aerosols to form cloud droplets and ice crystals and thus enables simulations of full aerosol indirect effects (Morris and Gettlemen, 2008), which was missing the model's predecessors.

The simulations used in this study are based on a model version of nominal 1º horizontal resolution (0.9º X 1.25º) and 30 vertical levels. All simulation outputs analyzed in this study are monthly data.

2.2 Existing simulations

Our study relies on two published large ensemble datasets using CESM1 (CAM5):

a. CESM1 Large Ensemble Project (CESM1-LENS; Kay et al., 2015);

b. CESM1 "Single Forcing" Large Ensemble Project (Deser et al., 2020).

The CESM1-LENS includes a 40-member ensemble of fully coupled simulations for the period of 1920-2100 with the same historical radiative forcing up to 2005 and the RCP8.5 scenario thereafter (Kay et al., 2015). Each ensemble member starts from the same simulation restart file in 1920 but with slightly different air temperatures perturbed at the level of round-off error. In this paper, we use "ALL" (i.e., all forcing considered) to represent this large ensemble. One advantage of having a large ensemble simulation is that we can separate climate responses to external forcings from internal variabilities by ensemble averaging. Thus, all results in this study are based on the ensemble average.

https://doi.org/10.5194/acp-2021-407
Preprint. Discussion started: 31 May 2021


Atmospheric Chemistry and Physics Discussions

The CESM1 "Single Forcing" Large Ensemble uses the same model setup of the CESM1-LENS but with individual external forcing fixed at the 1920 level while keeping all other external forcing evolving with time into the 21st century. The "Single Forcing" Large Ensemble includes four sets of ensembles with different single forcings fixed: (1) industrial aerosols (XAERindus, 20 members, 1920-2080), (2) biomass burning aerosols (XAERbmb, 15 members, 1920-2029), (3) greenhouse gases (XGHGs, 20 members, 1920-2080), and (4) land-use/land-cover (XLULC, 5 members, 1920-2029). Here in this study, we only used the first two ensembles. We changed the notation of the two ensembles to "Fix_FF1920" ("FF" stands for Fossil Fuel) and Fix_BB1920 ("BB" stands for Biomass Burning) because, in the emission inventory dataset, energy/transportation sector-related emission is also fixed, rather than the industrial activities only as the original notation implies. We also emphasize the timing (the year 1920) of leveling emission here because anthropogenic aerosol emissions in these simulations are not removed entirely but rather stay at a relatively low level (blue lines in Fig. 1 a and b).

By subtracting the "Fix_FF1920" or "Fix_BB1920" ensemble average results from the "ALL" ensemble, we can obtain climate responses to the Fossil-Fuel-related aerosol forcing (FF) or Biomass-Burning aerosol forcing (BB). Note that other sets of single forcing simulations (e.g., historicalMisc cases in CMIP5 (Taylor et al., 2012), and "hist-aer" cases in CMIP6) simulate only historical aerosol evolution with all other forcings fixed at pre-industrial state. The fix-aerosol method adopted here (as in Deser et al., 2020, but also in earlier studies such as Xu et al., 2015) serves to estimate the aerosol effects with all other external forcings (such as GHGs) evolving in the background, arguably an advantage in experimental design to assess the actual impact of single forcing.

One potential issue of using the fixed single forcing approach is that we have assumed additivity when differencing "ALL" and fixed single forcing cases (i.e., Fix_FF1920 or Fix_BB1920). The additivity assumption is examined in several recent studies focusing on the nonlinear interaction between aerosols and GHGs (Deng et al., 2020) and for various climate variables, in particular for extreme precipitation (Lin et al., in review). Furthermore, as in Deser et al., (2020), we consider the simple addition of FF response and BB response as the overall climate response to anthropogenic aerosol forcing (denoted as "AA"). Nevertheless, the focus of this study is on the contrasting role of FF and BB, motivated by the apparent difference in timing (blue vs. green lines in Fig. 1c, d) and emission locations (both in zonal and meridional directions).

2.3 New simulation

The existing two sets of single forcing large ensemble simulations (Fix_FF1920 and Fix_BB1920) enables a robust separation of aerosol-induced responses and a comparison of the role of FF and BB forcing. However, FF forcing features a strong zonal asymmetry starting from the 1980s (blue solid vs. dashed lines in Fig. 1 c, d), which continuously increases over

https://doi.org/10.5194/acp-2021-407
Preprint. Discussion started: 31 May 2021


Atmospheric Chemistry and Physics Discussions

the EH (dashed lines) and decreases over the WH (solid lines). The sharp contrast and competition between WH and EH in FF emission and forcing trend (driven by different air pollution policy) brings extra complexity to our attribution.

To gain further insights on the role of regional forcing (East vs. West), we conducted two additional sets of "regional" single forcing large ensemble simulations (10 realizations for each case) by branching from the existing run of Fix_FF1920. In the experiment of Fixed *Eastern* Fossil Fuel simulation (Fix_EastFF1920), we use the same initialization protocol as Fix_FF1920, but only fix the aerosols over the EH box (0–80 ºN, 60–150 ºE; shown as the blue dashed box in Fig. 2), where FF aerosol emissions over other regions are allowed to evolve, including the decline over North America and Europe (shown as the blue solid box in Fig. 2). The experiment of Fixed *Western* Fossil Fuel simulation (Fix_WestFF1920) is similar to the setup of Fix_EastFF1920 case except that we fix the aerosols over WH box (20º–80ºN, 130º–10ºW, and 30º–80ºN, 10ºW–40ºE; shown as the blue dashed box in Fig. 2). We run the two sets of simulations from 1920 through 1980 for one realization, and then expand the ensemble size to be 10 for 1980–2020. A small random perturbation of surface temperature is applied to each realization to generate ensemble spreads.

In Fix_EastFF1920, except for the strong cooling forcing in the lower latitudes of East Asia, a weak warming forcing over Siberia due to the extension of WH aerosol reduction is also included. However, the extended positive forcing is considerably weak compared to the negative forcing and is largely constrained in the small emission domain. Therefore, the difference between ALL and Fix_EastFF1920 can be safely used to represent the climate in response to the dominant role of the negative radiative forcing from lower latitudes of Asia.

Note that we did not conduct the analogous simulation for BB because, for NH, significant BB emission and forcing trends during 1980-2020 are only over the EH (green dashed lines in Fig. 1 c and d), specifically from Northeast Asia (blue oval in the right panel of Fig. 2). Thus, the existing Fix_BB1920 simulation already captures the regional contribution from the EH.

3 Results

3.1 Zonal asymmetry of anthropogenic aerosol forcing in the recent decades

Figure 1 shows the global and regional emissions of two major types of AA (sulfur aerosols and organic carbon). Globally, it is clear that the AA emission started to decline since the late 20th century (shaded area of 1980-2020 as the focused period of this study), but the decrease in aerosols mainly comes from developed countries in North America and Europe (solid lines as Western Hemisphere (WH) in Fig. 1c, d) while the developing countries in Asia (e.g., China and India) are still in the phase of increasing aerosol emission (dashed lines as Eastern Hemisphere (EH) in Fig. 1c, d).

https://doi.org/10.5194/acp-2021-407
Preprint. Discussion started: 31 May 2021


Atmospheric Chemistry and Physics Discussions

The 1st row of Fig. 2 depicts the 40-year linear trend of the SO4 column burden between 1980 and 2020. SO4 trend, as the dominant cooling aerosol produced by FF, shows a clear heterogeneous pattern in NH, with a decrease over North America and Europe (shown as the blue solid box) and a strong increase over China and India (shown as the blue dashed box).

Unlike Sulfate, another major cooling aerosol species, primary organic matter (POM) burden shows different distributions (2nd row of Fig. 2). FF-related POM is similar to that of SO4 burden but with much weaker negative trends over North America and also a weaker positive trend over China, compared to SO4. In contrast, BB-related POM features a much stronger increasing trend over northeastern Asia (40 ºN–70 ºN, 70 ºE–150 ºE), and a slight decrease over rain forests of Amazon and Congo. Combining FF and BB, the significant increasing trend of POM occurs over Asia at both low latitudes and high latitudes, while a relatively weaker decline trend can be found over Europe, Africa, and South America, again constituting a west-east zonal asymmetry. The Secondary Organic Aerosol (SOA) burden resembles the SO4 burden in both FF and BB cases but with weaker trends.

Aerosols with heating effects (such as Black Carbon; not shown) resemble the spatial pattern of SO4 burden shown in Fig. 2. However, the overall aerosols effect is dominated by cooling aerosols such as SO4. Thus, in this study, we only focus on the total cooling effect of aerosols, without separating the warming and cooling competition as done in several earlier studies (Xu and Xie, 2015; Lin et al., 2016; Wang et al., 2017).

Looking at aerosol mass burden only is insufficient to establish connections between the radiative forcing response and aerosol emissions because different aerosol species could have different radiative forcing efficiency. Thus, we further show Aerosol Optical Depth due to anthropogenic aerosol emission (AOD_AA) in the bottom panels of Fig. 2. To remove AOD induced by natural aerosols such as dust and sea salt, we derive AOD_AA following Eq. (1)1, in which, the AODVIS is the total AOD at the 550nm band, and the AODDUST 1-3 represent the dust AOD with different sizes. The background AOD (bkg_AOD) is the 100-year climatology of (AODVIS - AODDUST(1-3)) in the CESM1 pre-industrial control run, which is dominated by sea salt.

$$AOD_{AA} = AODVIS - AODDUST(1-3) - bkg.AOD\ , \quad (1)$$

As expected, the AOD_AA trend (third row in Fig. 2) in response to FF resembles the SO4 burden (first row in Fig. 2), while AOD_AA in responses to BB is in close agreement with the POM. Both FF and BB AOD trends feature zonal asymmetry across the Pacific ocean, with subtle differences in terms of latitudinal distribution (increase at lower latitudes versus decrease at higher latitudes in FF. The implications of these spatial contrasts on climatic responses will be further discussed in the next section.

https://doi.org/10.5194/acp-2021-407
Preprint. Discussion started: 31 May 2021


Atmospheric Chemistry and Physics Discussions

It is clear that BB shows a simple distribution without zonal competition, where a significant increase occurs over northeastern Asia. Therefore, our following discussion will only focus on the FF responses, which show subtle zonal differences. Based on the released simulation and the new regional-FF simulations, we are able to separate the climate responses in response to aerosol increase over EH and aerosol reduction over WH.

In line with the zonal asymmetry of AOD_AA trends, simulated solar radiation flux also has major zonal contrast, because of both direct and indirect climate effects of aerosols. The first row of Fig. 3 shows the Surface Downward Solar radiation (FSDS) which is largely consistent with the patterns of the AOD_AA trend (third row of Fig. 2). Note the opposite colors, though, because a decline in AOD_AA leads to an increase in FSDS. The global net radiative forcing shows an overall positive trend in response to the decrease in global sulfate emission, but with significant spatial heterogeneity due to the opposite regional emission trends. Different from AOD_AA changes which are concentrated over or near emission regions, FSDS changes are also seen over expanded regions due to the aerosol indirect effects, where the cloud droplet numbers and cloud lifetimes are enhanced by aerosols. This is corroborated by the Total Cloud fraction (CLDTOT, the second row of Fig. 3). CLDTOT in response to FF decreases over the North Atlantic, contributing to the significant enhancement of FSDS over NH high latitudes. The Pacific warm pool region in the and FF EastFF cases shows a strong increase in CLDTOT due to the strong local emission increase, and this leads to a strong negative trend in FSDS. Surprisingly, the Pacific warm pool also shows slight increase of CLDTOT in response to WestFF without local emission, which might be associated with the remote influence of WH forcing on the Pacific region.

The Net Solar Radiation at the Top-Of-Atmosphere (FSNTOA; third row of Fig. 3), as the main metric for aerosol forcing, is also consistent with FSDS patterns, showing positive global net radiative forcing trend. Interestingly, the North Pacific region shows complex competitions of the two emission sources, where WestFF induces a significant increase of FSNTOA (along with a decreasing CLDTOT) while EastFF leads to an opposite and weaker trend. Overall, the negative trend of FSNTOA due to EastFF is offset by WH forcing and leads to a slightly positive trend over this region. By only looking at the FF response over North Pacific, it is somewhat counter-intuitive: one may expect an increase in FF aerosol over Asia would lead to a negative forcing trend, but actually, the simulated negative trends are confined to lower latitude regions close to the emission source (blue oval in Fig. 2 bottom row left). But the two sets of regional forcing simulations reveal clearly that the decline of FF aerosol over the WH mid-latitudes (red oval in Fig. 2 bottom row right) dominates the North Pacific radiative forcings, producing a weak positive FSNTOA trend. This kind of East-West competition is a focal point of our analysis and we will further discuss the possible mechanisms later in terms of temperature and circulation changes in the subsequent sections.

https://doi.org/10.5194/acp-2021-407
Preprint. Discussion started: 31 May 2021


Atmospheric Chemistry and Physics Discussions

3.2 Simulated responses in the hemispheric average of surface air temperature

In Sect. 3.1, we demonstrate the distinct East-West pattern of the aerosol emission changes and its radiative effect. This section analyzes the simulated response in the hemispheric average of Surface Air Temperature (SAT).

Figure 4a shows the Northern Hemisphere (NH) mean SAT from the three large ensemble simulations. Without the FF aerosol emission in Fix_FF1920 simulation (blue line in Fig. 4a), NH-mean SAT is significantly warmer than the air temperature in the ALL simulation (black line in Fig. 4a). Large volcanic eruptions (Four major ones are shown as vertical dashed lines in Fig. 4a) also strongly affect the NH-mean SAT by causing abrupt cooling of about 0.1 to 0.3 K episodically but the cooling effects quickly recover in a few years, which means it hardly affects the multi-decadal climate trend. The global-mean SAT evolutions resemble the NH result but with a weaker magnitude. The stronger response over NH is reasonable because most of the emission sources (and land regions) are located at NH and aerosol burden and radiative forcing (Fig. 2 and 3) are regionally concentrated.

Fig. 4b shows the climate response to FF by calculating the difference between ALL and Fix_FF1920 simulation. It indicates that the mid-20th-century aerosol cooling effect is dominated by FF aerosol (Meehl et al., 2004; Diao and Xu., in review) with a cooling trend of 0.16 K/decade over NH. Since the 1980s, as the aerosol emission started to decline over WH, the NH-mean SAT response to FF aerosol has shifted to a slightly warming trend by about 0.07 K/decade.

Because of the distinct East-West aerosol forcing asymmetry, we further examine how the aerosol emissions would influence regional SAT differently. Fig. 4c–d shows the temperature responses over the Eastern (80 ºE–140 ºW) and the Western (90 ºW–30 ºE) portion of NH separately. The domains are shown as the red boxes in Fig. 3 but here we only have the NH portion to be considered to be consistent with Fig. 4a and b. The Western-NH temperature in response to FF (Fig. 4d) is largely following local emission evolution (Fig. 1), with a cooling along with the increasing emission before the 1980s and warming along with emission reduction afterward.

Notably, the Eastern-NH responses to FF are counter-intuitive: There is a warming trend of 0.06 K/decade (same as Western-NH) after the 1980s (Fig. 4c) even with continuously increasing aerosol emission over this region, suggesting that Eastern-NH is sensitive to the remote influence of WH aerosols. Indeed, the Eastern-NH cooling response is even larger than the Western-NH response during the previous cooling period (1940-1980; -0.17 K/decade versus -0.11 K/decade). The apparent contradiction of the EH warming in response to FF (Fig. 4c) and the local negative FF forcing (3rd row of Fig. 2) bears important implications on tropospheric temperature and circulation changes (to be further explored in Sect. 3.4). Here we argue that the larger remote response of EH temperature to WestFF is due to the latitudinal difference in aerosol emission location: WH emission changes mainly occur over mid-to-high latitudes (30–60ºN; the first row of Fig. 2), while the EH

https://doi.org/10.5194/acp-2021-407
Preprint. Discussion started: 31 May 2021


Atmospheric Chemistry and Physics Discussions

emission changes are mainly located over low-to-mid latitudes (below 40ºN, the first row of Fig. 2). As a result, during 1980-2020, there is only a weak regional cooling over EH, due to local FF aerosols and is confined over low latitudes of EH; but the WH decline of emission (positive forcing) dominates the mid-to-high latitudes SAT change, including North Pacific. Detailed analysis of this subtle latitudinal contrast in forcing (visualized in colored ovals in Fig. 2 bottom) will be provided in Sect. 3.4 for regional SAT over North Pacific.

3.3 Tropospheric responses

Because of the complex zonal and meridional differences in aerosol emission during 1980-2020 (Sect. 3.1), and the competition between EastFF and WestFF in changing NH air temperature (Sect. 3.2), tropospheric circulation responses could also be distinct over different regions. In this subsection, we discuss the global and regional tropospheric circulation responses due to the evolving anthropogenic aerosol emission, which have a major implication on mid-latitude extreme weather (Xu and Xie, 2015; Mann et al., 2017; Wang et al, 2020).

Previous studies have explored the tropospheric circulation responses to inter-hemispheric (meridional) forcing gradient due to anthropogenic aerosols – more reflecting aerosols over NH compared to SH will lead to an equatorward shift of NH Hadley circulation and NH westerly wind (e.g., Hwang et al., 2013; Hilgenbrink et al., 2018). However, from 1980 to 2020, NH anthropogenic aerosol forcing (Sect. 3.1) is highly heterogeneous, with strong zonal contrasts and subtle latitudinal differences (colored ovals at the bottom of Fig. 3), further compounding the forcing-response relationship. Next, we will analyze the aerosol-induced tropospheric responses (in terms of zonal average) both globally and regionally for the EH and WH portions (domains as red boxes in Fig. 3a).

Figure 5a–c shows the global Zonal Mean Meridional overturning Stream Function (ZMMSF) in contour plots in response to FF, EastFF, and WestFF, and the corresponding FSDS trend gradient in the line plot beneath the contour plots. The ZMMSF in response to FF features a counter-clockwise Hadley Cell anomaly (shown in blue) over the tropics, which indicates a northward shift of the Hadley Cell into NH with an increasing positive FSDS gradient (dash line in "FSDS gradient" panel). The northward shift of Hadley Cell also occurs in response to WestFF, but not to EastFF, indicating that the shift of Hadley Cell is mainly due to the WestFF, which induces warming over NH mid-latitudes and thus leading to a positive interhemispheric FSDS gradient. On the other hand, the EastFF forcing induces a slight negative FSDS gradient over the NH low latitudes, which fails to drive the shift of Hadley Cell. The global mean ZMMSF shifts in our results are consistent with previous studies (Xu et al., 2015; Allen and. Ajoku, 2016; Amaya et al., 2018; Shen et al., 2018) focusing on the inter-hemispheric forcing gradient. That is, the tropical circulation always tends to move towards a warmer hemisphere with larger positive forcing.

https://doi.org/10.5194/acp-2021-407
Preprint. Discussion started: 31 May 2021


Atmospheric Chemistry and Physics Discussions

Are NH mid-latitude jet streams changing consistently as tropical circulation? Figure 5d–f shows the global-mean zonal wind (U) trends. The FF and EastFF forcing induce a reduction of U speed on the poleward flank of the NH jet core and an increase of U speed on the equatorward flank of the jet core (especially in the EastFF case), which indicate the equatorward shifts of the NH jet stream (marked by red arrows in Fig. 5d–e). However, in the WestFF case, the. U speed on both sides of the jet core decreases (equatorward side greater than the poleward side) and the position of the jet core has no significant shift.

To summarize, the shift of NH jet stream in response to FF forcing is mainly controlled by the EastFF, but not WestFF. In contrast, as we discussed in the previous paragraph, the shift of the Hadley cell is mainly controlled by the WestFF. As a result, the shift of Hadley Cell and NH jet stream in FF case are in opposite directions, which appears to disagree with previous studies (Xu et al. 2015). However, based on the regional FF simulations (Fig 5b–c & e–f), we show that the jet stream and Hadley Cell in FF are controlled by opposite forcings during this period (cooling forcing induced by EastFF vs. warming forcing induced by WestFF), which agrees with the argument provided by Xu et al (2015). The competitions between EastFF and WestFF in shaping the Hadley Cell and mid-latitude Jet stream further indicate the importance of the meridional location of the aerosol forcings except for the zonal difference. Previous studies (Seo et al., 2014; Kang et al., 2020) also suggest the importance of latitudinal position of the radiative forcing to that the movement of tropical circulations, which is consistent with our findings here.

The latitudinal profiles under the contour plots in Fig. 5 d–f is the corresponding zonal mean FSNTOA gradient trend (black curves), which we argue provides rule-of-thumb guidance of the expected shift of NH jet stream. The FSNTOA gradient in response to FF and EastFF show an increase of FSNTOA gradient trend over the mid-latitudes (black dashed lines in Fig. 5), which tends to drive the equatorward shift of the NH jet stream. On the contrary, the FSNOTA gradient in WestFF slightly decreases with latitude, with no significant shift of NH jet stream. Actually, the FSNTOA gradients in FF and WestFF are similar although with a different latitudinal gradient (black dashed lines in Fig.5), which means that purely FSNTOA gradient cannot perfectly indicate the shift of NH jet stream. However, considering the consistent relationship between the shift of jet stream and the FSNTOA gradient, we argue that it can provide a simple and quick rule-of-thumb predictor of the expected shift of NH jet stream, and more precise mechanisms of the jet stream shift driven by FF forcings will be discussed later.

It's worth noting that in the line plots of Fig. 5, we adopt the latitudinal *gradient* of radiation flux trend (surface or TOA; in the unit of W/m^2/decade/10ºLat), rather than the actual trend. If we adopt the global mean forcing trend instead, it will suggest an opposite shifting direction of moving into the warmer side of the climatological jet stream (for example Fig. 5f), and thus would not serve well as a rule-of-thumb predictor. More fundamentally, it is the latitudinal gradient of forcing (i.e.

https://doi.org/10.5194/acp-2021-407
Preprint. Discussion started: 31 May 2021


Atmospheric Chemistry and Physics Discussions

warming or cooling rate) that drives the jet stream to change, not the local forcing, because it reflects the zonal component of the geostrophic wind equation, which is demonstrated next.

Figure 6a–c shows the zonal-mean geopotential wind in the zonal direction (Ug) in EH (red dashed box in Fig. 3), which is derived from geopotential height (Z) following the geostrophic wind equation. The derived Ug patterns always resemble the simulated U pattern in EH (Fig. 6d–f), WH, and Global (not shown), revealing the strong correlation between tropospheric circulation changes and the tropospheric temperature changes (and thus the geopotential height changes). Instead of the gradient of radiative variables as in Fig. 5, here we show the latitudinal profiles of the trend of SAT gradient in response to each force. It has been previously demonstrated that the tropospheric responses to sulfate aerosol are anchored to the SST gradient (Xu and Xie., 2015).

In EH, FF induces nearly no SAT gradient at low latitudes and positive gradients above 20 ºN (Fig. 6a), which is similar to WestFF. While on the other hand, EastFF induces a negative SAT gradient below 35 ºN. The sign of SAT gradient supports our previous argument that the jet stream changes are largely linked with Ug. The EastFF-induced SAT in NH has a slightly negative gradient on the equator flank of the NH jet core (below 35 ºN) and a positive SAT gradient on the polar flank (max at about 45 ºN), leading to a great strengthening of zonal wind on the equatorward flank of the jet core and weakening on the poleward flank. This is producing a net effect of an equatorward shift of NH jet (arrow in Fig. 6b), which is consistent with the results in Fig. 5. The WestFF- and FF-induced SAT does not show a negative gradient at low latitudes, and thus the zonal wind on the equatorward flank of the jet core does not increase significantly or continue to decrease but with smaller magnitude compared with the poleward flank. The WH jet stream changes are much weaker in comparison with the global-mean (Fig. 5d–f) and EH results (Fig. 6d–f) because the air temperature gradients are much weaker and thus are not shown in the figures.

To summarize, Fig. 6 shows that the local trend of SAT gradient well explains the weakening or strengthening of the NH jet stream following the geostrophic wind equation, while the latitudinal slope of the SAT gradient (dashed line as the linear fit in Fig. 6) indicates the shift of jet stream. A consistent governing principle emerging from Fig. 6 is that: NH jet stream always tends to shift towards the more negative portion of SAT gradient. This is consistent with Fig. 5 – NH jet stream always shifts towards the more negative portion of forcing gradient.

As shown in Fig. 4, the EH still experiences a warming tendency, the same as WH, in response to FF, despite an increasing aerosol emission locally at low-to-mid latitudes. So, to further reveal the contrast between EH and WH in response to FF as well as regional FF forcings, we re-assess the identified relationship between radiative forcing gradient, temperature gradient, and the tropical circulation changes in Fig. 5–6, by extracting the regional signals from the global mean states.

https://doi.org/10.5194/acp-2021-407
Preprint. Discussion started: 31 May 2021


Atmospheric Chemistry and Physics Discussions

Figure 7 (1st and 2nd rows) shows the regional ZMMSF and U changes relative to the global-mean state. The EH-Globe (EH minus global mean) and WH-Globe show opposite ZMMSF trends at low latitudes with opposite slopes of FSDS gradients in both the FF case and the regional FF cases, indicating the importance of radiative gradient *within* NH to govern the tropospheric circulation adjustment. In the low-to-mid latitudes of EH (5 ºN to 35 ºN), the gradient of the FSDS trend in response to FF is negative compared to the global-mean, which is largely consistent with the increasing aerosol emission in EH (3rd row of Fig. 2). The increasing FSDS gradient from south to north in NH leads to a clockwise ZMMSF trend and a poleward shift of Hadley Cell, which is consistent with the result shown in Xu and Xie (2015) and references within.

The relationship between the gradient of the SAT trend and the shift of the NH jet stream is re-assessed in the middle row of Fig. 7, in terms of regional anomalies over EH and WH relative to the global average. The results also support the simple relationship we identified in Fig. 5–6: the NH jet stream shifts to the flank with a more negative SAT gradient because the magnitude of U trend at certain latitudes is determined by the local gradient of air temperature trend, with a more negative gradient strengthening the westerly wind there. One Counterexample here is the WH-Globe U in response to WestFF, where jet stream does not shift even with a slight negative SAT gradient. The air temperature trend pattern (bottom row of Fig. 7) reveals that the negative gradient of air temperature locates at 30 ºN at all pressure levels, which is the latitude of the jet core. As a result, the jet core does not shift much as desired.

3.4 Surface temperature responses over the NH with a focus on North Pacific

Having demonstrated a coherent relationship between tropical circulation changes and that in radiation fluxes and SAT in Sect. 3.3, now we address the following apparent paradox in the FF case: relative to the global mean, EH mid-to-high latitudes have a positive SAT response despite an EH negative forcing, and similarly, WH mid-to-high latitudes have a negative T response (relative to the global mean) despite a local positive forcing (due to aerosol reduction; Fig. 3). Indeed, more than just SAT, EH mid-latitudes (45 ºN–60 ºN), relative to Global, also shows a warming tendency in tropospheric temperature below 250 hPa, which is contradictory to a local near zero external forcings (Fig. 7e). In contrast, when there is no WH external forcing in the Fix_EastFF1920 simulation, the EH mid-to-high latitudes show significant cooling response due to only EH aerosol forcing (Fig. 7f), which is mentioned by previous studies that demonstrate the north Pacific cooling due to Asia aerosol emissions. This suggests that the mid-to-high latitudes of EH is heavily influenced by WH external forcing, consistent with the hemispheric mean SAT trends shown in Sect. 3.2 and Fig. 4. Next, We provide further discussion of the mechanisms of tropospheric and surface air temperature adjustment in EH and WH.

The 1st row of Fig. 8 shows the 40-year linear trends of Surface Air Temperature (SAT) over the ocean in response to FF, EastFF, and WestFF, which bears a close similarity to SST (not shown). Overall, the FF forcing induces significant warming over the North Pacific above 40 ºN during 1980–2020, which is even stronger than the North Atlantic warming. The

https://doi.org/10.5194/acp-2021-407
Preprint. Discussion started: 31 May 2021


Atmospheric Chemistry and Physics Discussions

warming is inconsistent with the negative FF forcing at EH low-to-mid latitudes (marked by the blue oval in the middle left panel of Fig. 8), which only produces a weak local cooling over the western Pacific warm pool region. The SAT response to EastFF, unlike that to FF, shows significant cooling over the major part of North Pacific except for the east coast region above 50 North North Atlantic shows a warming trend in response to EastFF. On the other hand, the WestFF, with warming forcing at WH mid-to-high latitudes (30 ºN–60 ºN; marked by the red oval in the middle left panel of Fig. 8) induce es strong warming trend, inducing warming patterns not only locally at North Atlantic but more so over the North Pacific.

Comparing the three sets of responses. It is clear that the North Pacific warming trend above 40 ºN is more dominated by the remote forcing from WH mid-to-high latitudes due to aerosol emission reduction. The cooling responses to EastFF over the North Pacific below 40 ºN are offset by the remote warming response to WestFF. We also compared the BB response (not shown), which has cooling forcing over northeastern Asia over 50 ºN, and we find that BB-induced cooling occurs over the whole North Pacific just like WestFF does. Therefore, we further argue that the latitudinal distribution of aerosol forcing is important to the North Pacific climate responses, and this is why the high latitude regions of the North Pacific are dominated by WestFF but not EastFF.

The SAT response to EastFF also shows a PDO-like pattern (in positive phase), with cooling northwest Pacific and warming tropical Pacific. The WestFF induced SAT also shows dipole similar to negative-phase PDO pattern over the tropical and South Pacific but not North Pacific. Previous studies suggest that a transition into the negative PDO phase can be induced by industrial aerosol emissions emitted over Asia (Kaufmann et al., 2011; Newman et al., 2016; Smith et al., 2016) and have ramifications on the slowdown of global warming.

The competition of EastFF and WestFF over the North Pacific deserves some more discussion. The North Atlantic warming, as many other studies (e.g., Navarro et al., 2017) pointed out, can be attributed to the reduction of aerosol emission over North America and Europe starting since the 1980s, which is seen in TOA net energy flux (middle row of Fig. 8). However, the TOA net energy flux over the North Pacific region does not show any stronger positive forcing in FF and EastFF cases. In WestFF response, the FNTOA does show a positive trend over North Pacific but is significantly weaker than that over North Atlantic. This reveals that the response of radiative forcing to WestFF cannot fully explain the North Pacific warming. So why the stronger SST warming trend over North Pacific compared with North Atlantic? Intuitively, it seems that increasing aerosol emission over EH (notably China and India) could contribute to regional cooling. However, as shown in Sect. 2 and 3.3, there is a clear contradiction between FF aerosol emission increase and regional-mean warming over the North Pacific. Previous studies also shared similar conclusions, arguing that Atlantic SST is more tightly controlled by local aerosol-induced radiation change (Boo 2015; Navarro et al., 2017), while North Pacific SST can be more affected by atmospheric circulation changes induced by external forcing and/or internal Atlantic variations (Qin 2020).

https://doi.org/10.5194/acp-2021-407
Preprint. Discussion started: 31 May 2021


Atmospheric Chemistry and Physics Discussions

So how does WH forcing lead to North Pacific warming (and also in the tropospheric circulations of EH mid-to-high latitudes in Fig. 7)? zonal mean meridional heat transport (ZMMHT, the third row of Fig. 8), over WH shows a positive trend above 60 ºN (note that the climatology of ZMMHT over both North Pacific and North Atlantic are still positive in poleward direction, as shown in line contour of Fig. 8 bottom). This suggests that the meridional energy transfer from the Atlantic Ocean to the Arctic is enhanced, slowing down the North Atlantic warming rate due to local aerosol positive forcing. Conversely, North Pacific ZMMHT (poleward in climatology) is weakened and thus exports less heat from North Pacific mid-latitudes to the polar region (blue color in the EH panels of Fig. 8). This explains why the North Pacific shows a stronger warming trend even without local emission change or local forcing. Comparing WestFF and EastFF, it is clear that the WestFF forcing is the dominating driver of the equatorward meridional heat transport othe ver North Pacific. Another possible explanation for the stronger North Atlantic warming is that the mid-latitude region of EH is controlled by the WH emission reduction effects at mid-to-high latitudes via the zonal energy transport between the Atlantic and Pacific (McGregor et al., 2014).

To summarize, the simulated North Pacific warming above 50 ºN is dominating by the WestFF forcing at mid-to-high latitudes. The EastFF forcing at low-to-mid latitudes, which are extensively discussed by previous studies, induces cooling trend at mid latitudes (below 50 ºN) over North Pacific, which is similar to the positive PDO-like response, but the signal is overwhelmed by the warming tendency induced by WestFF, via both radiative forcing response and meridional heat transport from pole region.

4 Summary

The main findings of this paper are:

(1) In terms of aerosol forcing, the Eastern Hemisphere (EH) and the Western Hemisphere (WH) show very different anthropogenic aerosol emission trends since the 1980s, where WH started to reduce Fossil Fuel (FF) emission in comparison to the continuous increasing in both FF and BB emission over EH (Fig. 1 and Fig. 2). Due to FF, positive forcing occurs at mid to high latitudes (above 30 ºN) and negative forcing occurs over low latitude regions (particularly West tropical Pacific ocean and Indian ocean). Due to BB, negative forcing mainly occurs close to the emission domain (Northeastern Asia) with some extension to the North Pacific (Fig. 3). The major zonal contrast in aerosol emission redistribution, and to a less extent the latitudinal difference, leads to opposite local radiative forcing that has competing effects on regional climate.

(2) In terms of hemispheric surface temperature response: the overall FF emission decreases since the 1980s, mostly driven by the WH, induces a significant warming trend over NH. Interestingly, although the FF emission over EH

https://doi.org/10.5194/acp-2021-407
Preprint. Discussion started: 31 May 2021


Atmospheric Chemistry and Physics Discussions

continuously increases, the SAT in EH still shows a warming trend as large as WH, because of the heavy influence from WH aerosol reduction.

(3) In terms of tropospheric circulation responses: in response to FF, NH shows an overall positive gradient of temperature trend (cooling low latitude, warming high latitude), inducing a counterclockwise anomaly (i.e., a poleward shift) of Hadley and an equatorward shift of NH jet stream (Fig. 5). Previous studies show that the shift of mid-latitude jet stream is associated with the SST meridional gradient, and a cooling NH drives an equatorward shift of both Hadley Cell and NH jet stream (Xu and Xie, 2015; Xu et al., 2016), which appears to be inconsistent with our results. The main difference is that previous results are largely based on a sharp interhemispheric forcing gradient with a time scale of the entire 20th century (Wang et al., 2020), or focusing on the mid-century era where global aerosol emission is on the rise (Diao and Xu, in review).

In this study, with a focus on the period of 1980–2020, the regional FF forcing competitions within the NH is more complex given that the EH and WH show heterogeneous distributions in both zonal and meridional direction, and even opposite trends (an increase of aerosol emission over EH versus reduction over WH). The competitions between EH and WH are illustrated with two sets of separate large ensemble simulations (Fix_EastFF1920 and Fix_WestFF1920) we conducted. Our result shows that the poleward shift of Hadley Cell is controlled by the WestFF forcing at mid-to-high latitudes, while the equatorward shift of NH jet stream is mainly driven by EastFF forcing at low-to-mid latitudes. The competitions between EastFF and WestFF in shaping the Hadley Cell and mid-latitude Jet stream indicate the key role of the meridional distribution of the aerosol forcings.

The gradient of surface downward solar flux (FSDS) provides a rule-of-thumb guidance of the expected shift of the NH jet stream (Fig. 7). It is because the jet stream patterns largely agree with the geostrophic wind (Ug) patterns (Fig. 6), which are derived from the latitudinal gradient of air temperature. The NH jet stream always tends to shift to the negative gradient portion of FSDS.

(4) In terms of North Pacific temperature response, the FF forcing during 1980-2020, unlike suggested by previous studies, induces North Pacific and pan-Pacific warming due to a competition between EastFF and WestFF, with the latter dominating the former (Fig. 8). The dominance is due to the latitudinal distribution of aerosol forcing within the NH. The negative forcing of EastFF, which occurs at the EH tropical and subtropical region (0–40 ºN), is largely confined to the emission domain. In contrast, negative FF forcing over WH mid-to-high latitudes (above 30 ºN), not only introduces local warming but also imposes a heavy influence over North Pacific warming. Diagnostic shows that the remote contribution to North Pacific warming from WestFF is due to the combination of both radiative forcing responses and meridional energy transfer anomaly from the North Atlantic to North Pacific via the Arctic pathway.

The importance of the inter-hemispheric asymmetry of external forcing has been extensively discussed in previous studies (e.g., Xu et al., 2015; Chung et al., 2017; Wang et al., 2020), in which the NH is usually considered as a whole. Here we

https://doi.org/10.5194/acp-2021-407
Preprint. Discussion started: 31 May 2021


Atmospheric Chemistry and Physics Discussions

further emphasize that the latitudinal difference of external forcing within the NH is important in determining the tropospheric and surface responses. More specifically, The EastFF induces a PDO-like pattern (negative phase) with a cooling over the northwestern Pacific and warming over the tropical Pacific. However, when combined with the aerosol reduction over the WH, the EastFF-driven northwestern Pacific cooling is completely offset and instead exhibits a warming trend.

We provide the following discussions related to our conclusion and suggest some future research directions.

(1) The issue of nonlinearity. The CESM1 single forcing large ensemble simulations applied in this study treats the FF and BB forcing separately, which enables many of our discussions above. However, one problem is the additivity of the two anthropogenic aerosol sources. Deser et al. (2020) sum up the FF, BB, and GHGs responses to reconstruct the all forcing (ALL) response, and find some inconsistencies due to the nonlinear interactions between aerosol- and GHG-induced responses. So, it is also possible that adding FF and BB may cause some nonlinear problems. Similarly, adding EastFF and WestFF responses may also cause such problems. This study is not affected by such additivity problems because we treat each set of simulations separately, but future studies that aim to utilize the combined AA-induced changes, should be cautious and a rigorous test on additivity would be necessary.

(2) The issue of RCP8.5 scenarios applied in CESM1. As is described in Sect. 2.1, the RCP8.5 scenarios are applied in all five sets of large ensemble simulations used in this study for 2006-2020. Studies have pointed out that the RCP dataset is different from the new SSP scenarios which contain the historical emission data up to 2015. For example, the sulfate emissions over India and China over the 2006-2020 period in the RCP8.5 scenarios are lower than observations and SSP scenarios, which could lead to an underestimate of the sulfate cooling effects locally and globally (Lin et al., 2018). Future experiments utilizing the newer GCMs and SSP scenarios would be helpful to repeat and test the current results.

(3) The single model large ensemble method. The single model large ensemble simulations applied in this study effectively separate the external forcing induced response from the model internal variability (Kay et al., 2015; Deser, et al., 2020). However, one limitation here is that only one GCM is utilized, so the potential systematic errors from a single model cannot be tested. Some new single-forcing large ensemble simulations based on models other than CESM1 (e.g., CanESM2 (Oudar et al., 2018); CESM2) are also coming out recently as part of the "Single Model Initial-condition Large Ensemble" (SMILE) efforts, which brings the possibility of testing "multi-model large ensemble" in future works and improving our understanding of aerosol induced climate change.

(5) The implication of North Pacific response on the PDO mode and global warming rate. The increasing FF emission over EH low latitudes (without WH) induce a PDO-like SAT response over the North Pacific and tropical Pacific, suggesting

https://doi.org/10.5194/acp-2021-407
Preprint. Discussion started: 31 May 2021


Atmospheric Chemistry and Physics Discussions

the potential impact of anthropogenic forcing onto the internal variability. More future research is needed on this topic based on the current large ensemble simulations and the upcoming CESM2 simulations.

(6) The subtle difference of EastFF and WestFF in the north-south direction. It is clear that the redistribution of anthropogenic aerosol since 1980s is not a pure zonal shift, but also shifts in the meridional direction. The aerosol loading shows a net decrease, especially in the mid-latitude/subpolar region. Future studies may consider both zonal and meridional shifts in SO4 loading.

https://doi.org/10.5194/acp-2021-407
Preprint. Discussion started: 31 May 2021

Atmospheric Chemistry and Physics Discussions

References

Acosta Navarro, J. C., Ekman, A. M. L., Pausata, F. S. R., Lewinschal, A., Varma, V., Seland, Ø., Gauss, M., Iversen, T., Kirkevåg, A., Riipinen, I., and Hansson, H. C.: Future Response of Temperature and Precipitation to Reduced Aerosol Emissions as Compared with Increased Greenhouse Gas Concentrations, 30, 939–954, https://doi.org/10.1175/JCLI-D-16-0466.1, 2017.

Allen, R. J., Norris, J. R., and Kovilakam, M.: Influence of anthropogenic aerosols and the Pacific Decadal Oscillation on tropical belt width, Nat. Geosci., 7, 270–274, https://doi.org/10.1038/ngeo2091, 2014.

Allen, R. J. and Ajoku, O.: Future aerosol reductions and widening of the northern tropical belt, J. Geophys. Res. Atmos., 121, 6765–6786, https://doi.org/10.1002/2016JD024803, 2016.

Allen, R. J., Turnock, S., Nabat, P., Neubauer, D., Lohmann, U., Olivié, D., Oshima, N., Michou, M., Wu, T., Zhang, J., Takemura, T., Schulz, M., Tsigaridis, K., Bauer, S. E., Emmons, L., Horowitz, L., Naik, V., van Noije, T., Bergman, T., Lamarque, J.-F., Zanis, P., Tegen, I., Westervelt, D. M., Le Sager, P., Good, P., Shim, S., O'Connor, F., Akritidis, D., Georgoulias, A. K., Deushi, M., Sentman, L. T., John, J. G., Fujimori, S., and Collins, W. J.: Climate and air quality impacts due to mitigation of non-methane near-term climate forcers, Atmos. Chem. Phys., 20, 9641–9663, https://doi.org/10.5194/acp-20-9641-2020, 2020.

Amaya, D. J., Siler, N., Xie, S.-P., and Miller, A. J.: The interplay of internal and forced modes of Hadley Cell expansion: lessons from the global warming hiatus, Clim. Dyn., 51, 305–319, https://doi.org/10.1007/s00382-017-3921-5, 2018.

Andreae, M. O., Jones, C. D., and Cox, P. M.: Strong present-day aerosol cooling implies a hot future, Nature, 435, 1187–1190, https://doi.org/10.1038/nature03671, 2005.

Bahadur, R., Praveen, P. S., Xu, Y., and Ramanathan, V.: Solar absorption by elemental and brown carbon determined from spectral observations, Proc. Natl. Acad. Sci., 109, 17366–17371, https://doi.org/10.1073/pnas.1205910109, 2012.

Bellomo, K., Murphy, L. N., Cane, M. A., Clement, A. C., and Polvani, L. M.: Historical forcings as main drivers of the Atlantic multidecadal variability in the CESM large ensemble, Clim. Dyn., 50, 3687–3698, https://doi.org/10.1007/s00382-017-3834-3, 2018.

Bender, F. A.-M.: Aerosol Forcing: Still Uncertain, Still Relevant, AGU Adv., 1, e2019AV000128, https://doi.org/10.1029/2019AV000128, 2020.

Booth, B. B. B., Dunstone, N. J., Halloran, P. R., Andrews, T., and Bellouin, N.: Aerosols implicated as a prime driver of twentieth-century North Atlantic climate variability, Nature, 484, 228–232, https://doi.org/10.1038/nature10946, 2012.

Dai, A., Fyfe, J. C., Xie, S. P., and Dai, X.: Decadal modulation of global surface temperature by internal climate variability, Nat. Clim. Chang., 5, 555, https://doi.org/10.1038/nclimate2605, 2015.

Deng, J., Dai, A., and Xu, H.: Nonlinear Climate Responses to Increasing CO2 and Anthropogenic Aerosols Simulated by CESM1, J. Clim., 33, 281–301, https://doi.org/10.1175/JCLI-D-19-0195.1, 2019.

600 Deser, C., Phillips, A. S., Simpson, I. R., Rosenbloom, N., Coleman, D., Lehner, F., Pendergrass, A. G., DiNezio, P., and Stevenson, S.: Isolating the Evolving Contributions of Anthropogenic Aerosols and Greenhouse Gases: A New CESM1 Large Ensemble Community Resource, J. Clim., 33, 7835–7858, https://doi.org/10.1175/JCLI-D-20-0123.1, 2020.

Ding, Q., Schweiger, A., L'Heureux, M., Steig, E. J., Battisti, D. S., Johnson, N. C., Blanchard-Wrigglesworth, E., Po-Chedley, S., Zhang, Q., Harnos, K., Bushuk, M., Markle, B., and Baxter, I.: Fingerprints of internal drivers of Arctic sea ice
605 loss in observations and model simulations, Nat. Geosci., 12, 28–33, https://doi.org/10.1038/s41561-018-0256-8, 2019.

Hilgenbrink, C. C. and Hartmann, D. L.: The Response of Hadley Circulation Extent to an Idealized Representation of Poleward Ocean Heat Transport in an Aquaplanet GCM, J. Clim., 31, 9753–9770, https://doi.org/10.1175/JCLI-D-18-0324.1, 2018.

Hua, W., Dai, A., and Qin, M.: Contributions of Internal Variability and External Forcing to the Recent Pacific Decadal
610 Variations, Geophys. Res. Lett., 45, 7084–7092, https://doi.org/10.1029/2018GL079033, 2018.

Hua, W., Dai, A., Zhou, L., Qin, M., and Chen, H.: An Externally Forced Decadal Rainfall Seesaw Pattern Over the Sahel and Southeast Amazon, Geophys. Res. Lett., 46, 923–932, https://doi.org/10.1029/2018GL081406, 2019.

IPCC: IPCC Special Report on the impacts of global warming of 1.5°C, Ipcc - Sr15, 2018.

Jacobson, M. Z.: Investigating cloud absorption effects: Global absorption properties of black carbon, tar balls, and soil dust
615 in clouds and aerosols, J. Geophys. Res. Atmos., 117, https://doi.org/10.1029/2011JD017218, 2012.

Kaufmann, R. K., Kauppi, H., Mann, M. L., and Stock, J. H.: Reconciling anthropogenic climate change with observed temperature 1998–2008, Proc. Natl. Acad. Sci., 108, 11790 LP – 11793, https://doi.org/10.1073/pnas.1102467108, 2011.

Kay, J. E., Deser, C., Phillips, A., Mai, A., Hannay, C., Strand, G., Arblaster, J. M., Bates, S. C., Danabasoglu, G., Edwards, J., Holland, M., Kushner, P., Lamarque, J.-F., Lawrence, D., Lindsay, K., Middleton, A., Munoz, E., Neale, R., Oleson, K.,
620 Polvani, L., and Vertenstein, M.: The Community Earth System Model (CESM) Large Ensemble Project: A Community Resource for Studying Climate Change in the Presence of Internal Climate Variability, Bull. Am. Meteorol. Soc., 96, 1333–1349, https://doi.org/10.1175/BAMS-D-13-00255.1, 2015.

Kirtman, B., Power, S. B., Adedoyin, A. J., Boer, G. J., Bojariu, R., Camilloni, I., Doblas-Reyes, F., Fiore, A. M., Kimoto, M., Meehl, G., Prather, M., Sarr, A., Schar, C., Sutton, R., van Oldenborgh, G. J., Vecchi, G., and Wang, H.-J.: Chapter 11 -
625 Near-term climate change: Projections and predictability, in: Climate Change 2013: The Physical Science Basis. IPCC Working Group I Contribution to AR5, edited by: IPCC, Cambridge University Press, Cambridge, 2013.

Klimont, Z., Smith, S. J., and Cofala, J.: The last decade of global anthropogenic sulfur dioxide: 2000–2011 emissions, Environ. Res. Lett., 8, 14003, https://doi.org/10.1088/1748-9326/8/1/014003, 2013.

Kodros, J. K., Scott, C. E., Farina, S. C., Lee, Y. H., L'Orange, C., Volckens, J., and Pierce, J. R.: Uncertainties in global
630 aerosols and climate effects due to biofuel emissions, Atmos. Chem. Phys., 15, 8577–8596, https://doi.org/10.5194/acp-15-8577-2015, 2015.

Krishnan, S., Ekman, A. M. L., Hansson, H.-C., Riipinen, I., Lewinschal, A., Wilcox, L. J., and Dallafior, T.: The Roles of the Atmosphere and Ocean in Driving Arctic Warming Due to European Aerosol Reductions, Geophys. Res. Lett., 47, e2019GL086681, https://doi.org/10.1029/2019GL086681, 2020.

Lin, L., Gettelman, A., Xu, Y., and Fu, Q.: Simulated responses of terrestrial aridity to black carbon and sulfate aerosols, J. Geophys. Res. Atmos., 121, 785–794, https://doi.org/10.1002/2015JD024100, 2016.

Lin, L., Xu, Y., Wang, Z., Diao, C., Dong, W., and Xie, S.-P.: Changes in Extreme Rainfall Over India and China Attributed to Regional Aerosol-Cloud Interaction During the Late 20th Century Rapid Industrialization, Geophys. Res. Lett., 45, 7857–7865, https://doi.org/10.1029/2018GL078308, 2018.

Liu, D., He, C., Schwarz, J. P., and Wang, X.: Lifecycle of light-absorbing carbonaceous aerosols in the atmosphere, npj Clim. Atmos. Sci., 3, 40, https://doi.org/10.1038/s41612-020-00145-8, 2020.

Liu, X., Easter, R. C., Ghan, S. J., Zaveri, R., Rasch, P., Shi, X., Lamarque, J.-F., Gettelman, A., Morrison, H., Vitt, F., Conley, A., Park, S., Neale, R., Hannay, C., Ekman, A. M. L., Hess, P., Mahowald, N., Collins, W., Iacono, M. J., Bretherton, C. S., Flanner, M. G., and Mitchell, D.: Toward a minimal representation of aerosols in climate models: description and evaluation in the Community Atmosphere Model CAM5, Geosci. Model Dev., 5, 709–739, https://doi.org/10.5194/gmd-5-709-2012, 2012.

Mann, M. E., Rahmstorf, S., Kornhuber, K., Steinman, B. A., Miller, S. K., and Coumou, D.: Influence of Anthropogenic Climate Change on Planetary Wave Resonance and Extreme Weather Events, Sci. Rep., 7, 45242, https://doi.org/10.1038/srep45242, 2017.

McGregor, S., Timmermann, A., Stuecker, M. F., England, M. H., Merrifield, M., Jin, F.-F., and Chikamoto, Y.: Recent Walker circulation strengthening and Pacific cooling amplified by Atlantic warming, Nat. Clim. Chang., 4, 888–892, https://doi.org/10.1038/nclimate2330, 2014.

Meehl, G. A., Hu, A., Arblaster, J. M., Fasullo, J., and Trenberth, K. E.: Externally Forced and Internally Generated Decadal Climate Variability Associated with the Interdecadal Pacific Oscillation, J. Clim., 26, 7298–7310, https://doi.org/10.1175/JCLI-D-12-00548.1, 2013.

Meehl, G. A., Washington, W. M., Ammann, C. M., Arblaster, J. M., Wigley, T. M. L., and Tebaldi, C.: Combinations of Natural and Anthropogenic Forcings in Twentieth-Century Climate, J. Clim., 17, 3721–3727, https://doi.org/10.1175/1520-0442(2004)017<3721:CONAAF>2.0.CO;2, 2004.

Meehl, G. A., Hu, A., and Teng, H.: Initialized decadal prediction for transition to positive phase of the Interdecadal Pacific Oscillation, Nat. Commun., 7, https://doi.org/10.1038/ncomms11718, 2016.

Ming, Y. and Ramaswamy, V.: A Model Investigation of Aerosol-Induced Changes in Tropical Circulation, J. Clim., 24, 5125–5133, https://doi.org/10.1175/2011JCLI4108.1, 2011.

Newman, M., Alexander, M. A., Ault, T. R., Cobb, K. M., Deser, C., Di Lorenzo, E., Mantua, N. J., Miller, A. J., Minobe, S., Nakamura, H., Schneider, N., Vimont, D. J., Phillips, A. S., Scott, J. D., and Smith, C. A.: The Pacific Decadal Oscillation, Revisited, J. Clim., 29, 4399–4427, https://doi.org/10.1175/JCLI-D-15-0508.1, 2016.

Oudar, T., Kushner, P. J., Fyfe, J. C., and Sigmond, M.: No Impact of Anthropogenic Aerosols on Early 21st Century Global Temperature Trends in a Large Initial-Condition Ensemble, Geophys. Res. Lett., 45, 9245–9252, https://doi.org/https://doi.org/10.1029/2018GL078841, 2018.

Polvani, L. M., Previdi, M., England, M. R., Chiodo, G., and Smith, K. L.: Substantial twentieth-century Arctic warming caused by ozone-depleting substances, Nat. Clim. Chang., 10, 130–133, https://doi.org/10.1038/s41558-019-0677-4, 2020.

Qin, M., Dai, A., and Hua, W.: Aerosol-forced multidecadal variations across all ocean basins in models and observations since 1920, Sci. Adv., 6, eabb0425, https://doi.org/10.1126/sciadv.abb0425, 2020.

Samset, B. H., Myhre, G., Forster, P. M., Hodnebrog, Ø., Andrews, T., Faluvegi, G., Fläschner, D., Kasoar, M., Kharin, V., Kirkevåg, A., Lamarque, J.-F., Olivié, D., Richardson, T., Shindell, D., Shine, K. P., Takemura, T., and Voulgarakis, A.: Fast and slow precipitation responses to individual climate forcers: A PDRMIP multimodel study, Geophys. Res. Lett., 43, 2782–2791, https://doi.org/10.1002/2016GL068064, 2016.

Shen, Z. and Ming, Y.: The Influence of Aerosol Absorption on the Extratropical Circulation, J. Clim., 31, 5961–5975, https://doi.org/10.1175/JCLI-D-17-0839.1, 2018.

Shindell, D. T., Faluvegi, G., Rotstayn, L., and Milly, G.: Spatial patterns of radiative forcing and surface temperature response, J. Geophys. Res. Atmos., 120, 5385–5403, https://doi.org/doi:10.1002/2014JD022752, 2015.

Smith, D. M., Booth, B. B. B., Dunstone, N. J., Eade, R., Hermanson, L., Jones, G. S., Scaife, A. A., Sheen, K. L., and Thompson, V.: Role of volcanic and anthropogenic aerosols in the recent global surface warming slowdown, Nat. Clim. Chang., 6, 936–940, https://doi.org/10.1038/nclimate3058, 2016.

Swart, N. C., Fyfe, J. C., Hawkins, E., Kay, J. E., and Jahn, A.: Influence of internal variability on Arctic sea-ice trends, Nat. Clim. Chang., 5, 86–89, https://doi.org/10.1038/nclimate2483, 2015.

Verma, T., Saravanan, R., Chang, P., and Mahajan, S.: Tropical Pacific Ocean Dynamical Response to Short-Term Sulfate Aerosol Forcing, J. Clim., 32, 8205–8221, https://doi.org/10.1175/JCLI-D-19-0050.1, 2019.

Wang, H., Xie, S.-P., Zheng, X.-T., Kosaka, Y., Xu, Y., and Geng, Y.-F.: Dynamics of Southern Hemisphere Atmospheric Circulation Response to Anthropogenic Aerosol Forcing, Geophys. Res. Lett., 47, e2020GL089919, https://doi.org/10.1029/2020GL089919, 2020.

Wang, Y., Jiang, J. H., and Su, H.: Atmospheric responses to the redistribution of anthropogenic aerosols, J. Geophys. Res. Atmos., 120, 9625–9641, https://doi.org/10.1002/2015JD023665, 2015.

Wang, Y., Le, T., Chen, G., Yung, Y. L., Su, H., Seinfeld, J. H., and Jiang, J. H.: Reduced European aerosol emissions suppress winter extremes over northern Eurasia, Nat. Clim. Chang., https://doi.org/10.1038/s41558-020-0693-4, 2020.

Wang, Z., Lin, L., Yang, M., Xu, Y., and Li, J.: Disentangling fast and slow responses of the East Asian summer monsoon to reflecting and absorbing aerosol forcings, Atmos. Chem. Phys., 17, 11075–11088, https://doi.org/10.5194/acp-17-11075-2017, 2017.

Watanabe, M. and Tatebe, H.: Reconciling roles of sulphate aerosol forcing and internal variability in Atlantic multidecadal climate changes, Clim. Dyn., 53, 4651–4665, https://doi.org/10.1007/s00382-019-04811-3, 2019.

700 Xie, S.-P. and Kosaka, Y.: What Caused the Global Surface Warming Hiatus of 1998–2013?, Curr. Clim. Chang. Reports, 3, 128–140, https://doi.org/10.1007/s40641-017-0063-0, 2017.

Xu, Y. and Xie, S.-P.: Ocean mediation of tropospheric response to reflecting and absorbing aerosols, Atmos. Chem. Phys., 15, 5827–5833, https://doi.org/10.5194/acp-15-5827-2015, 2015.

Xu, Y., Lamarque, J. F., and Sanderson, B. M.: The importance of aerosol scenarios in projections of future heat extremes, 705 https://doi.org/10.1007/s10584-015-1565-1, 2018.

Zhao, A., Bollasina, M. A., and Stevenson, D. S.: Strong Influence of Aerosol Reductions on Future Heatwaves, Geophys. Res. Lett., 46, 4913–4923, https://doi.org/10.1029/2019GL082269, 2019.

Zheng, Y., Zhang, Q., Tong, D., Davis, S. J., and Caldeira, K.: Climate effects of China's efforts to improve its air quality, Environ. Res. Lett., 15, 104052, https://doi.org/10.1088/1748-9326/ab9e21, 2020.

710

https://doi.org/10.5194/acp-2021-407
Preprint. Discussion started: 31 May 2021

Atmospheric Chemistry and Physics Discussions

Figures

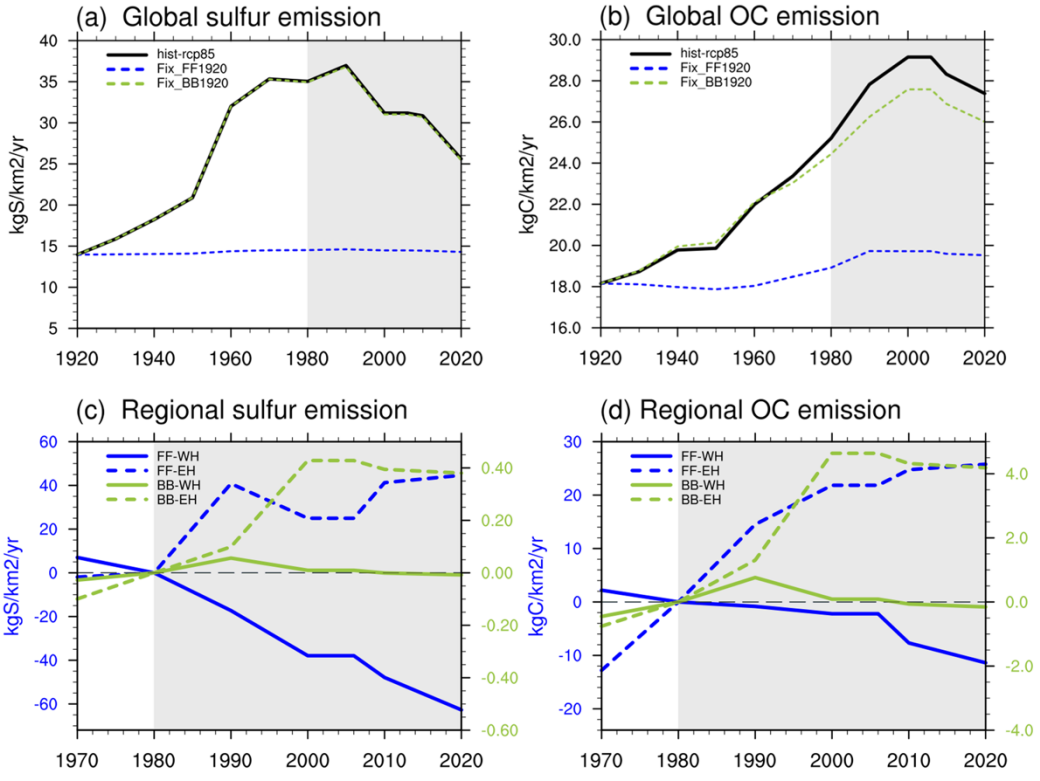

Figure 1:

(a) & (b): The global average anthropogenic emission of Sulfur and OC from 1920 to 2020 in the three sets of simulations used in this study. The "FF" represents the emission-related to Fossil Fuels. The "BB" represents Biomass Burning. Shading areas of 1980-2020 are the focused period.

(c) & (d): Similar to (a) & (b) but as the difference between ALL and corresponding fixed aerosol experiments to show the regional FF or BB emission. FF (blue lines) uses the left-hand side Y-axis and BB (green lines) uses the right-hand side Y-axis. Solid lines are for the "Western box" (West-box; 0-80°N, 120°W-40°E), and dashed lines are for the "Eastern box" (East-box; 0-80°N, 60°E-150°E). Boxes are shown in Fig. 2. All numbers in (c) and (d) are relative to the 1980 level to illustrate the change from 1980 to 2020.

https://doi.org/10.5194/acp-2021-407
Preprint. Discussion started: 31 May 2021

Atmospheric Chemistry and Physics Discussions

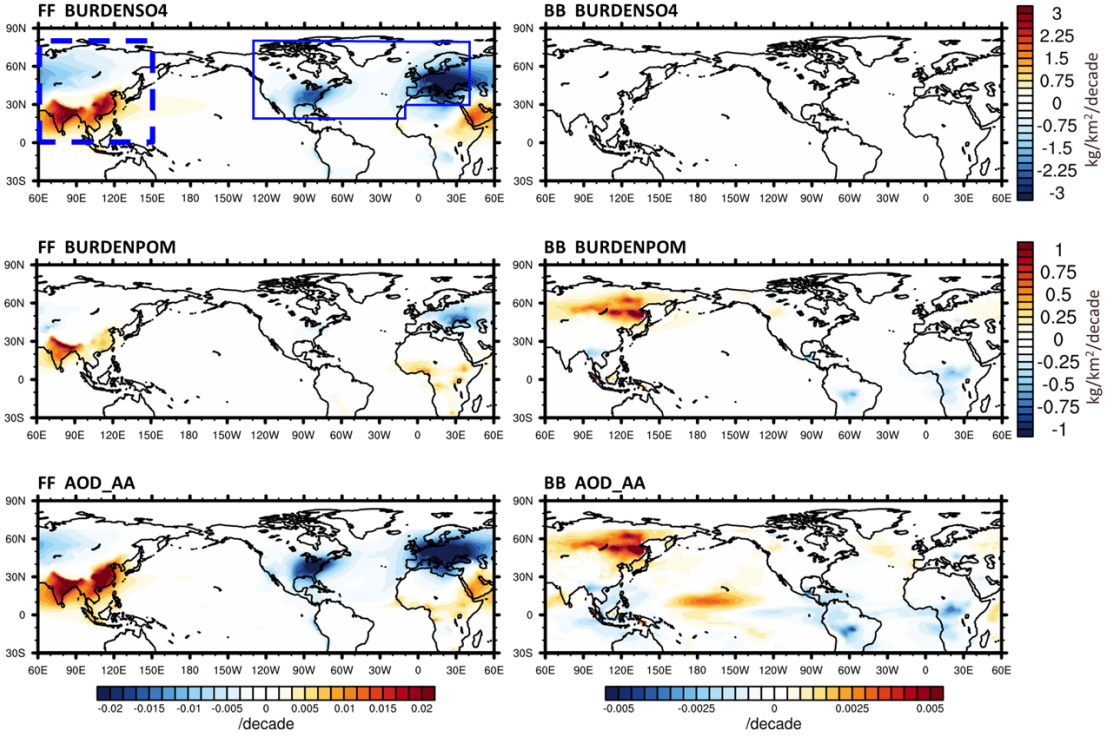

Figure 2:

1st & 2nd row : 40-year trend of Sulfate and Primary OC (POM) column burden (kg/km2/decade) in response to FF (left), and BB (right) emission changes. BC and SOA are not shown but the patterns are very similar to SO4.

3rd row: 40-year trend of AOD-AA (aerosol optical depth due to anthropogenic aerosols). Note the color scale of FF is twice of BB.

The blue dashed box in the upper left panel indicates the "Eastern Hemisphere" box (EH-box, 0°–80°N, 60°–150°E) used for the regional fixed-aerosol simulations. The solid box indicates the "Western Hemisphere" box (WH-box, 20°–80°N, 130°–10°W, and 30°–80°N, 10°W–40°E).

https://doi.org/10.5194/acp-2021-407
Preprint. Discussion started: 31 May 2021

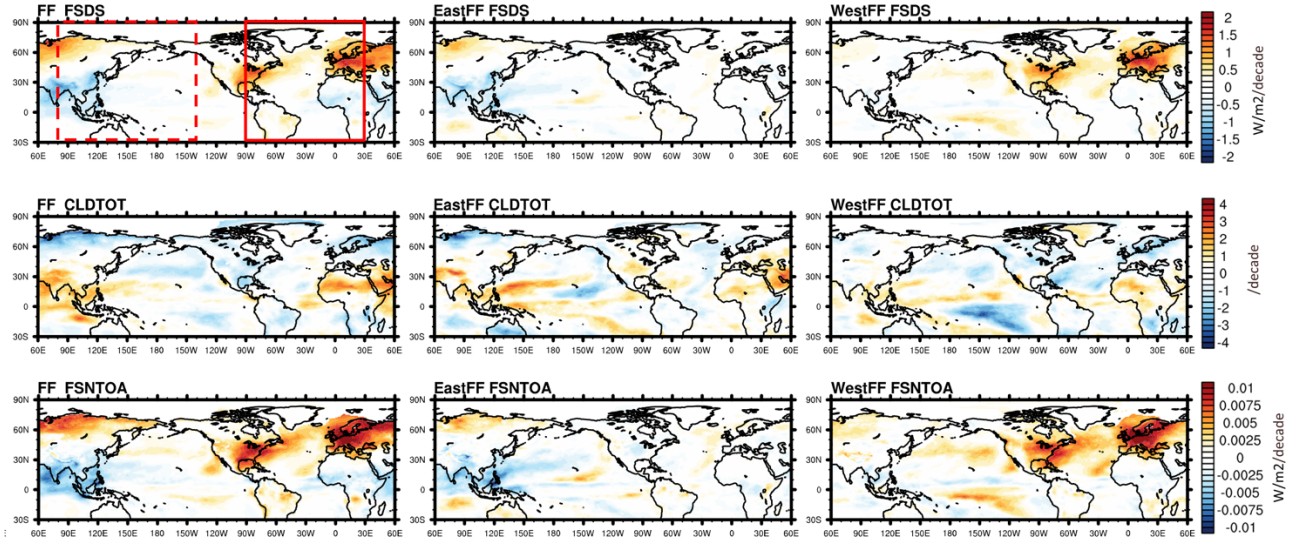

Figure 3:

(1st row) 40-year trend in surface downward solar flux (FSDS, W/m2/decade) in response to FF (left), EastFF (mid), and WestFF (right); (2nd row) Total cloud fraction (CLDTOT, 1/decade); and (3rd row) Top-of-Atmosphere net solar flux (FSNTOA, W/m2/decade).

Dotted areas indicate the region where the trend passes the 95% significance test

The high latitude ocean regions with significant sea ice change (e.g. the Arctic and the Sea of Okhotsk) are masked to remove the surface albedo change effects.

The dashed box in the left panel of 1st row indicates the "Eastern Hemisphere" (EH, 80°E-140°W) used in our subsequent analysis, and the solid box indicates the "Western Hemisphere" (WH, 90°W-30°E).

https://doi.org/10.5194/acp-2021-407
Preprint. Discussion started: 31 May 2021

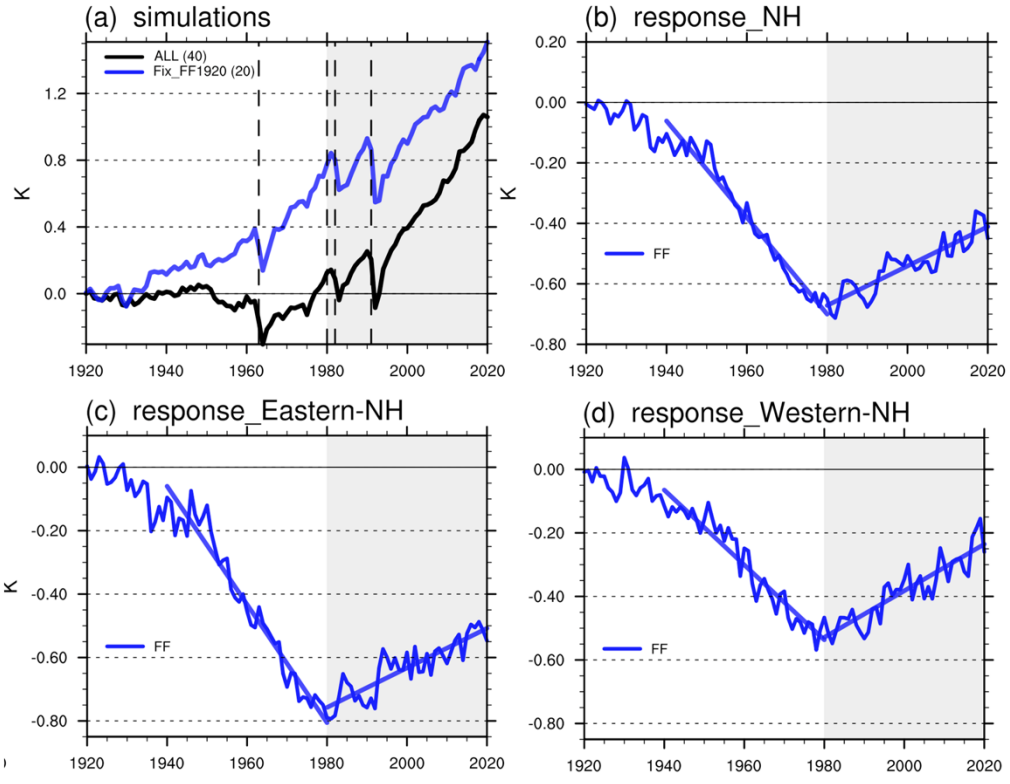

Figure 4:

(a) The Northern Hemisphere (NH) surface air temperature (SAT) anomalies (relative to 1920) in the three sets of simulations: ALL (all forcing: historical+RCP8.5) (black line; 40-member), and Fix_FF1920 (blue line; 20-member). The four dashed lines indicate the four major volcanic eruption events (greater than category 5) during the 20th century. Shaded areas are the focused period of this study.

(b) The SAT responses to FF (blue). The thinker straight lines indicate the 40-year linear fits for 1940-1980 and 1980-2020 respectively. (c) & (d) are similar to (b) but for the eastern part of NH and western part of NH (see boxes in Fig. 3).

https://doi.org/10.5194/acp-2021-407
Preprint. Discussion started: 31 May 2021

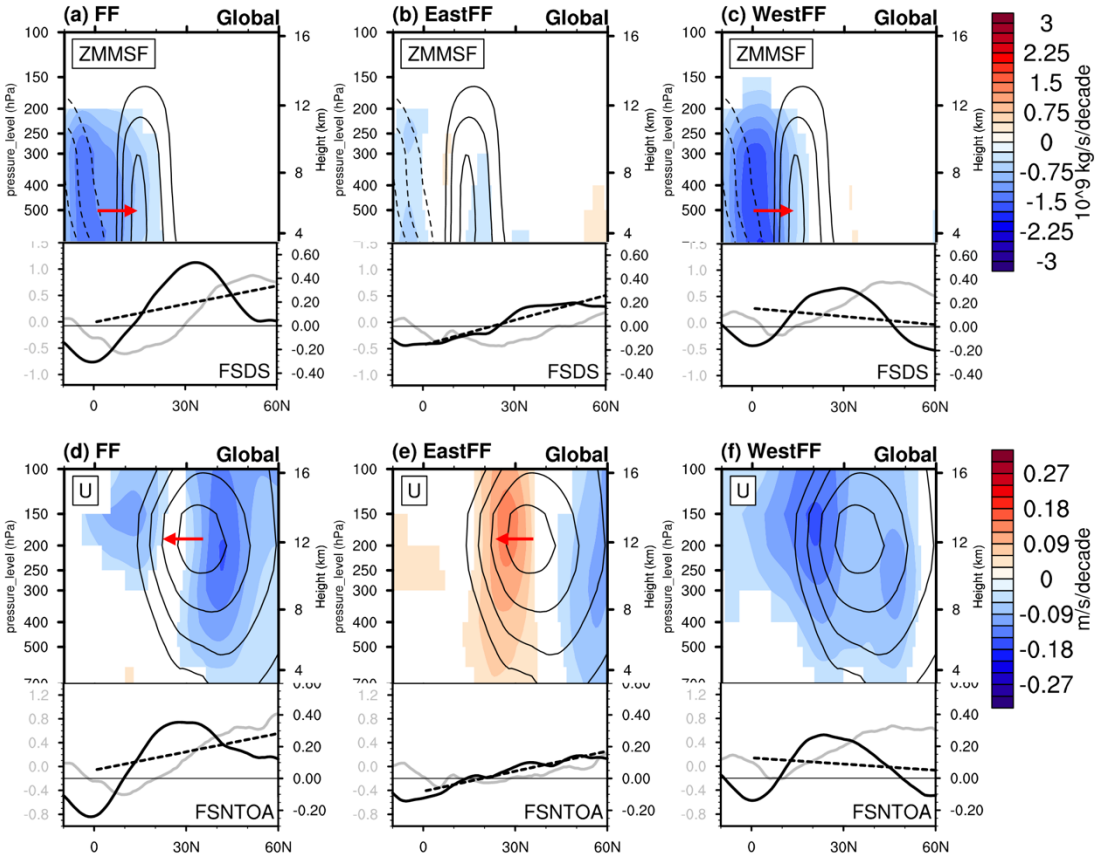

Figure 5:

(a–c) The 1980-2020 trend of zonal mean meridional stream function (ZMMSF, 10^9 kg/s/decade) in response to (a) FF, (b) EastFF, and (c) WestFF. The positive values (solid lines for climatology and red shading for long-term trend) indicate clockwise circulation.

The latitudinal profiles below show surface downward solar flux trend (FSDS as shown in Fig. 3; grey curves; W/m²/decade/), and its latitudinal gradient (FSDS_gradient; black curves; W/m²/decade/10°lat) smoothed in 30 degrees of latitudinal range, in which positive gradient indicates a larger FSDS trend at higher NH latitude. The dashed lines are the linear fit from 0° to 60°N.

The arrows indicate the latitudinal shift of Hadley cells.

(d–f) Similar to (a–c) but for zonal mean zonal wind (U, m/s/decade). The positive values indicate westerly wind. The statistically insignificant trend is masked in white. The latitudinal profiles below show the Top-of-Atmosphere net solar flux trend (FSNTOA as in Fig. 4c; W/m²/decade), and its latitudinal gradient (FSNTOA gradient; W/m²/decade/10°lat).

The arrows indicate the latitudinal shift of NH Jetstream core.

https://doi.org/10.5194/acp-2021-407
Preprint. Discussion started: 31 May 2021

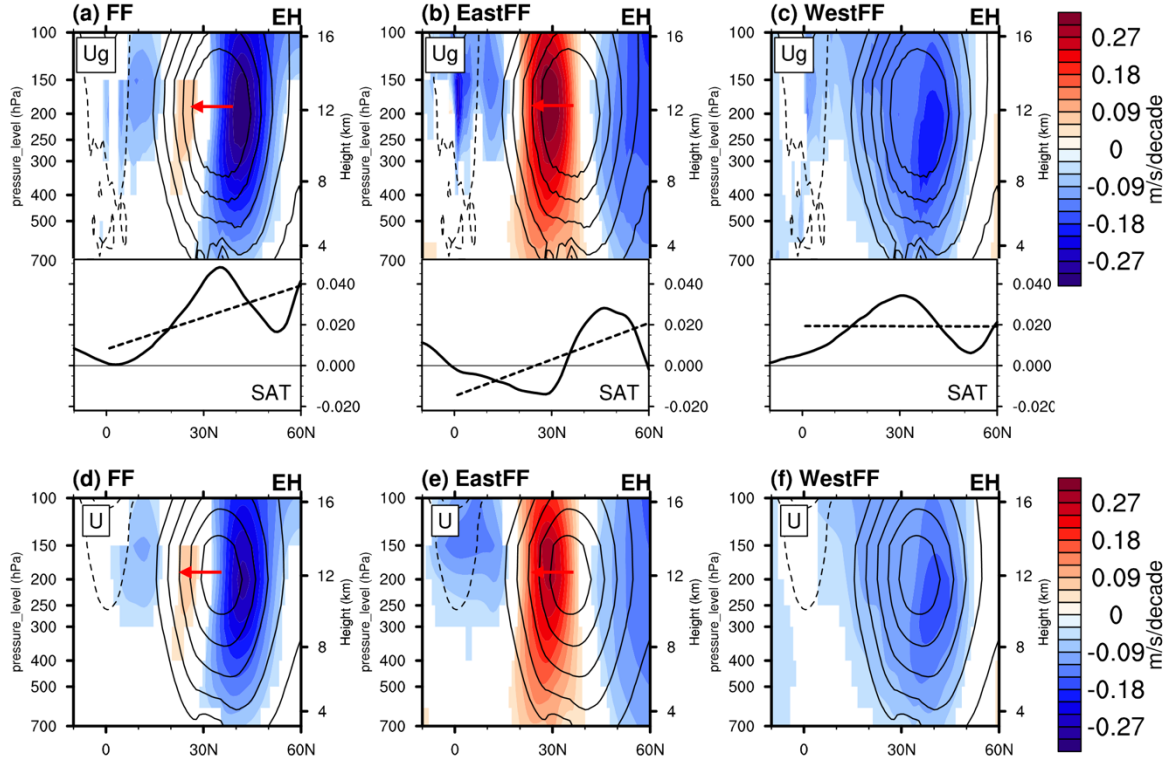

Figure 6:

(a–c) Similar to Fig. 6 (d–f) but for geostrophic wind (Ug) trend (m/s/decade) derived from geopotential height (Z) during 1980-2020 in Eastern Hemisphere (EH). The climatology is shown in contour lines with an interval of 6. The arrows indicate the latitudinal shift in each case.

The latitudinal profiles below show the gradient of surface air temperature (SAT) trend (smoothed in 30 degrees of latitudinal range; in unit of K/decade/10 ºlat). Positive values indicate a larger SAT trend at higher latitude, and vice versa. The dashed lines are the linear fit from 0º to 60ºN.

(d–f) Similar to Fig. 6 (d–f) but for U trend in Eastern Hemisphere (EH).

https://doi.org/10.5194/acp-2021-407
Preprint. Discussion started: 31 May 2021

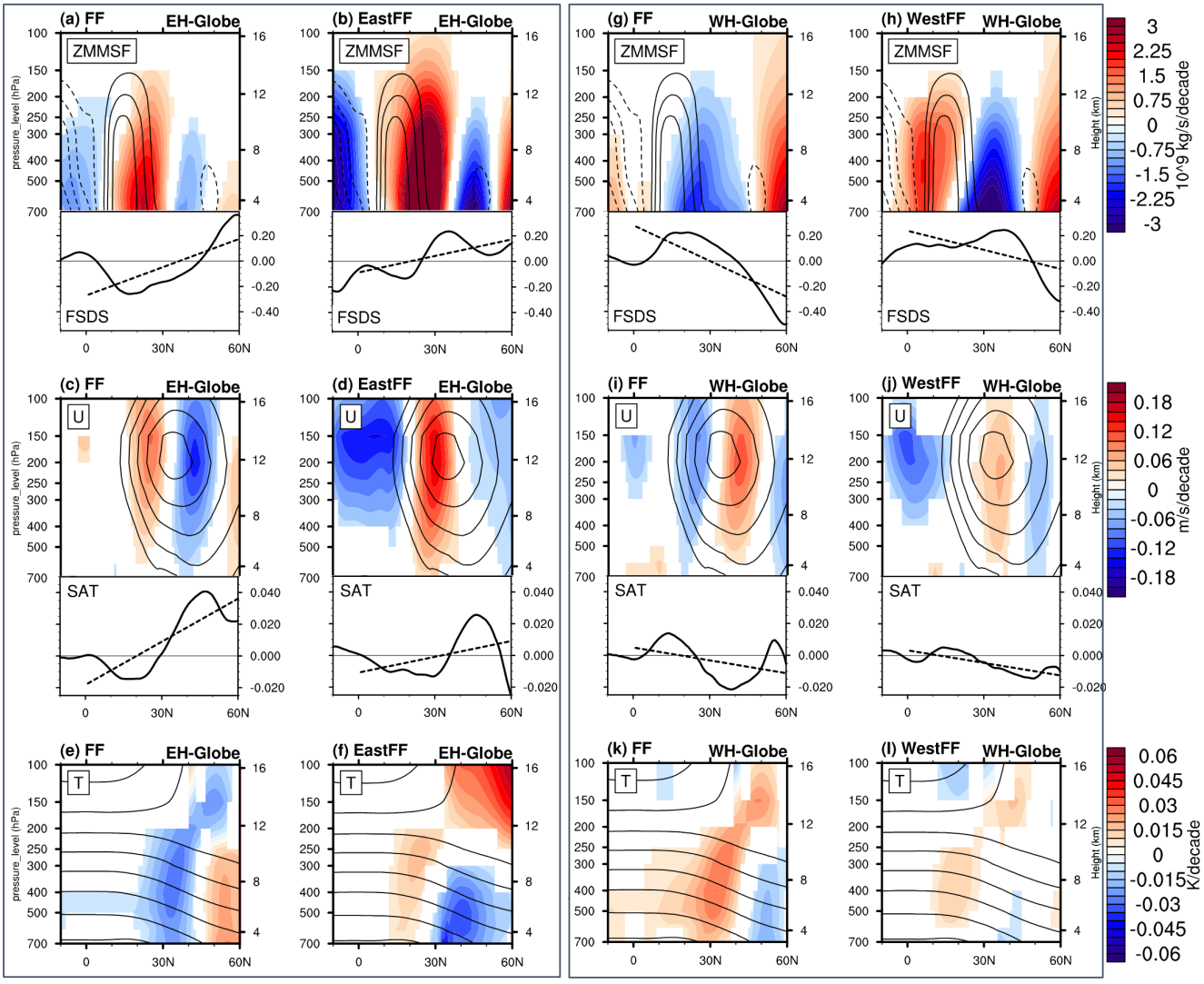

Figure 7:

1st row: ZMMSF trend, Same as Fig. 5 (a–c) but showing the difference between global mean and EH mean (a–b), and the difference between global mean and WH mean (g–h). The latitudinal profiles below show the latitudinal gradient of FSDS trend, which is also calculated as the difference between EH/WH and Globe.

2nd row: U trend, Same as Fig. 6 (d–f) but showing the difference between global mean and EH (WH). The latitudinal profiles below show the latitudinal gradient of SAT trend, which is also calculated as the difference between EH/WH and Globe.

3rd row: Similar to the above two rows but showing tropospheric air temperature (T) trend

https://doi.org/10.5194/acp-2021-407
Preprint. Discussion started: 31 May 2021

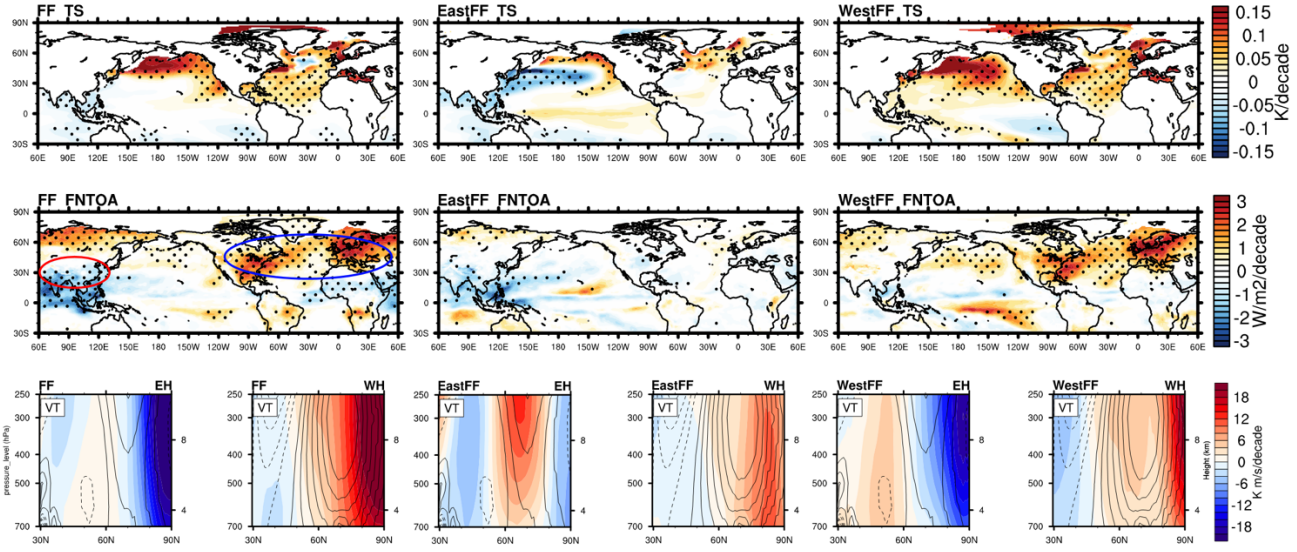

Figure 8:

1st & 2nd rows: 40-year trends of Sea surface air temperature (SSAT), and that of net energy flux at TOA (including shortwave and longwave, not FSNTOA shown in Fig. 4). Arctic regions in with significant sea ice changes are masked.

790 **The blue (red) circles in the 2nd row indicate the regions with significant decline (increase) of aerosol emission.**

3rd row: zonal mean of meridional heat transport (ZMMHT) in EH and WH. The positive values (solid lines for climatology and red shading for long-term trend) indicate poleward transfer. The arrows indicate the energy transfer responses relative to the climatology.

795